SCIENTIFIC REPORTS

OPEN

Received: 9 March 2017
Accepted: 6 June 2017
Published online: 18 July 2017

Heteroborospherene clusters $Ni_n \in B_{40}$ (n = 1–4) and heteroborophene monolayers $Ni_2 \in B_{14}$ with planar heptacoordinate transition-metal centers in η^7-B_7 heptagons

Hai-Ru Li, Xin-Xin Tian, Xue-Mei Luo, Miao Yan, Yue-Wen Mu, Hai-Gang Lu & Si-Dian Li

With inspirations from recent discoveries of the cage-like borospherene B_{40} and perfectly planar $Co \in B_{18}^-$ and based on extensive global minimum searches and first-principles theory calculations, we present herein the possibility of the novel planar $Ni \in B_{18}$ (1), cage-like heteroborospherenes $Ni_n \in B_{40}$ (n = 1–4) (2–5), and planar heteroborophenes $Ni_2 \in B_{14}$ (6, 7) which all contain planar or quasi-planar heptacoordinate transition-metal (phTM) centers in η^7-B_7 heptagons. The nearly degenerate $Ni_2 \in B_{14}$ (6) and $Ni_2 \in B_{14}$ (7) monolayers are predicted to be metallic in nature, with $Ni_2 \in B_{14}$ (6) composed of interwoven boron double chains with two phNi centers per unit cell being the precursor of cage-like $Ni_n \in B_{40}$ (n = 1–4) (2–5). Detailed bonding analyses indicate that $Ni_n \in B_{40}$ (n = 1–4) (2–5) and $Ni_2 \in B_{14}$ (6, 7) possess the universal bonding pattern of $\sigma + \pi$ double delocalization on the boron frameworks, with each phNi forming three lone pairs in radial direction ($3d_{z2}^2$, $3d_{zx}^2$, and $3d_{yz}^2$) and two effective nearly in-plane 8c-2e σ-coordination bonds between the remaining tangential Ni 3d orbitals ($3d_{x2-y2}$ and $3d_{xy}$) and the η^7-B_7 heptagon around it. The IR, Raman, and UV-vis absorption spectra of 1–5 are computationally simulated to facilitate their experimental characterizations.

Buckminsterfullerene C_{60} and its precursor graphene have been superstars in chemistry and materials science ever since their discoveries[1,2]. As the light neighbor of carbon, boron has a rich chemistry dominated with multi-center two-electron bonds (*mc-2e* bonds) in both bulk allotropes and polyhedral molecules to compensate for its electron-deficiency[3]. Multicenter bonds also appear to be responsible for the planar or quasi-planar (2D) structures of an unprecedentedly wide range of boron clusters $B_n^{-/0}$ (n = 3−30, 35, 36) characterized in gas phase in the past decade, unveiling a flat world of boron analogous to polycyclic aromatic hydrocarbons[4–18]. The possibility of all-boron fullerenes was not considered until 2007 when the high-symmetry I_h B_{80} cage was constructed from C_{60} by capping the twenty hexagons[19]. However, this celebrated structure was later found to be much less stable than its core-shell rivals at various density functional theory (DFT) levels[20,21]. The first all-boron fullerenes D_{2d} $B_{40}^{-/0}$, referred to as borospherenes in literature, were discovered in 2014 in a combined experimental and theoretical investigation[22]. In stark contrast to C_{60} which consists of twenty hexagons and twelve pentagons, D_{2d} B_{40} features four equivalent B_7 heptagons with large cavities on the waist which may serve as effective ligands to coordinate transition metal centers. The first axially chiral borospherenes C_3/C_2 B_{39}^- with three/four B_7 heptagons were observed in 2015[23]. In the past two years, the B_n^q (q = n−40) borospherene family has been expanded at first-principles theory level to include the cage-like B_{41}^+, B_{42}^{2+}[24], B_{40}^+[25], B_{38}^{2-} (in $Ca@B_{38}$)[26], B_{37}^{3-} (in $Ca@B_{37}^-$)[27], and B_{36}^{4-} (in $Li_4\&B_{36}$)[28] which are all composed of twelve interwoven boron double chains (BDCs) with six hexagonal and heptagonal faces on thesurface. These borospherenes follow the universal bonding pattern of

Institute of Molecular Science, Shanxi University, Taiyuan, 030006, China. Hai-Ru Li and Xin-Xin Tian contributed equally to this work. Correspondence and requests for materials should be addressed to Y.-W.M. (email: ywmu@sxu.edu.cn) or H.-G.L. (email: luhg@sxu.edu.cn) or S.-D.L. (email: lisidian@sxu.edu.cn)

$\sigma + \pi$ double delocalization. Endohedral and exohedral charge-transfer complexes M@B_{40} (M = Ca, Sr, La, Y, Sc) and M&B_{40} (M = Be, Mg) were also predicted to be stable species[29,30]. The experimentally observed quasi-planar $B_{36}^{-/0}$ and B_{35}^{-} clusters with one or two adjacent hexagonal vacancies appeared to be molecular motifs of infinite 2D borophene monolayers[9,10]. The first 2D borophene monolayers deposited on Ag(111) substrates were successfully synthesized by two independent groups in 2015[31,32]. Interestingly, the most stable χ^3-borophene deposited on Ag(111) is composed of zigzag BDCs in alternation with columns of adjacent hexagonal vacancies[32], further indicating the importance of BDCs in low-dimensional boronanostructures. A boron monolayer with octagons, heptagons, and hexagons was recently considered to be a 2D structural precursor of the B_{40} cage[33] though it is not a stable low-energy 2D polymorph compared to the well-known boron α-sheet and other low-lying structures[33–36]. Buckled FeB_2 and FeB_6 monolayers were recently proposed to be stable species with hexa-, hepta-, and octa-coordinate Fe centers[37,38]. Furthermore, the recent observation of the perfectly planar C_{2v} Co∈B_{18}^{-} with a planar heptacoordinate Co center opened vast opportunities to design 2D heteroborophene monolayers[39] and other heteroboronanostructures with planar or quasi-planar heptacoordinate transition-metal (phTM) centers. However, to the best of our knowledge, cage-like heteroborospherenes with phTM centers on the surface and stable heteroborophene monolayers as precursors of such heteroborospherenes have not been reported in either experiments or theory.

Based on extensive global minimum (GM) searches and first-principles theory calculations, we predict herein the existence of the perfectly planar heteroborophene-type cluster Ni∈B_{18} (**1**), cage-like heteroborospherenes Ni_n∈B_{40} (n = 1–4) (**2**–**5**), and the nearly degenerate heteroborophene monolayers Ni_2∈B_{14} (**6**, **7**) which all contain phNi centers in η^7-B_7 heptagons on the boron frameworks, with Ni_2∈B_{14} (**6**) composed of interwoven BDCs being the structural precursor of the cage-like Ni_n∈B_{40} (n = 1–4) (**2**–**5**). These heteroboronanostructures possess the universal bonding pattern of $\sigma + \pi$ double-delocalization on the boron frameworks, with each phNi center forming two effective 8c-2e σ-coordination bonds with the η^7-B_7 heptagon around it, inheriting the structural and bonding characteristics of the experimentally observed cage-like B_{40}[22] and perfectly planar Co∈B_{18}^{-}[39].

Computational procedures. Extensive GM searches were performed using both the Minima Hopping (MH)[40,41] and TGmin[42] algorithms on NiB_{18} and Ni_nB_{40} clusters (n = 1–2), in combination with manual structural constructions based on the low-lying isomers of CoB_{18}^{-}[39] and $B_{40}^{-/0}$[22]. Low-lying structures were then fully optimized with frequencies checked at both PBE0[43] and TPSSh[44] levels with the 6–311 + G* basis set[45] to ensure they are all true minima of the systems. The relative energies were further refined at the more accurate CCSD(T)[46–48] level with 6–31 G* basis set for the five lowest-lying isomers of NiB_{18} and NiB_{40}. A general global search based on the PSO technique implemented in the Crystal Structure Analysis by Particle Swarm Optimization (CALYPSO)[49] package was performed on 2D Ni_2B_{14} monolayer. The underlying plane-wave based DFT structrual optimization were performed using the Vienna *ab initio* simulation package (VASP)[50,51], within the framework of projector augmented wave (PAW) pseudopotential method[52,53] and PBE generalized gradient approximation (GGA)[54]. The Heyd−Scuseria−Ernzerhof (HSE06) approach[55] was used to calculate the band structures and densities of states of the PBE structures.

Results and Discussions

Structures and Stabilities of Heteroborospherenes. As expected from chemical intuition, the perfectly planar neutral C_{2v} Ni∈B_{18} (**1**) which is isovalent with the experimentally known C_{2v} Co∈B_{18}^{-}[39] turns out to be the global minimum of the cluster at CCSD(T) level (Fig. 1 and Fig. S1), with the Ni center and the η^7-B_7 heptagon around it matching nicely both geometrically and electronically. The existence of a planar Ni∈B_7 coordination unit in Ni∈B_{18} (**1**) presents the possibility of forming Ni-B binary nanostructures with phNi centers in η^7-B_7 heptagons. Given the fact that the experimentally observed borospherene D_{2d} B_{40} possesses four quasi-planar B_7 heptagons on the waist[22], it is reasonable to expect that D_{2d} B_{40} may serve as an effective ligand with four quasi-planar η^7-B_7 coordination sites to accommodate phNi centers on the cage surface. It turns out to be true. As indicated in Fig. 1a, Figs S3, and S4, both the cage-like C_s Ni∈B_{40} (**2**) and C_2 Ni_2∈B_{40} (**3**) are the global minima of the systems, while C_s Ni_3∈B_{40} (**4**) and D_{2d} Ni_4∈B_{40} (**5**) are true minima. All the phNi centers in the Ni_n∈B_{40} series (n = 1–4) (**2**–**5**) form effective Ni-B coordination interactions with the η^7-B_7 heptagons around them, as indicated by the average Ni-B distance of $\bar{r}_{Ni-B}$ = 2.02 Å in these clusters which is only slightly longer than the sum (1.95 Å) of the recommended single-bond covalent radii of Ni and B[56]. The twenty low-lying isomers of NiB_{40} all possess cage-like geometries, with the second (C_1) and third (C_{2v}) lowest-lying isomers lying about 0.41 eV higher than C_s Ni∈B_{40} (**2**) at PBE0 (Fig. S3). The C_2 Ni_2∈B_{40} (**3**) with two phNi centers in two neighboring B_7 heptagons lies 0.12 eV lower than the second lowest-lying C_{2v} Ni_2∈B_{40} which possesses two phNi centers at the opposite sites of the cage (Fig. S4). All the other isomers of Ni_2B_{40} lie at least 0.42 eV higher than Ni_2∈B_{40} (**3**) at PBE0. As shown in Fig. S5, the relative stabilities of the most concerned low-lying isomers are found to remain unchanged with Gibbs free energy corrections included at finite temperatures below 600 K. Interestingly, the coordination energies (E_c) of the Ni_n∈B_{40} (n = 1–4) series (**2**–**5**) with respect to $Ni_nB_{40} = Ni_{(n-1)}B_{40} + Ni$ (n = 1–4) (referring to triplet Ni and singlet Ni_nB_{40} in gas phases) increase almost perfectly linearly with the number of Ni atoms in the systems, with the large average E_c of 95.90 kcal/mol (4.16 eV/Ni) at PBE0 (Fig. 1b). The E_c~n linear relation indicates that the four η^7-B_7 heptagons in D_{2d} B_{40} can be practically viewed as four independent coordination sites to accommodate phNi centers. In comparison, the hexacoordinate Ni centers in Ni_5∈B_{40} (**8**) and Ni_6∈B_{40} (**9**) at the top and bottom of the B_{40} cage (Fig. S2) possess obviously lower average coordination energies (E_c = 75.54 kcal/mol) (Fig. 1b), indicating that phTM centers are favored over hexacoordinate transition-metal centers in the formation of heteroborospherenes. Ni_n∈B_{40} (n = 1–4) (**2**–**5**) have the large HOMO-LUMO energy gaps of 2.85 eV, 2.59 eV, 2.39 eV, and 2.32 eV at PBE0 level, respectively, well supporting their high chemical stabilities. Similar heteroborospherenes with phPd and phPt centers have also been obtained (Fig. S6).

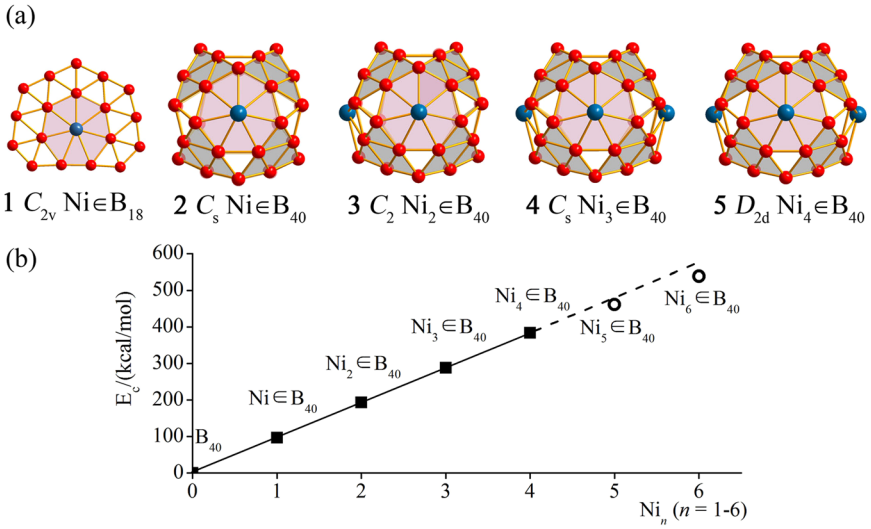

Figure 1. Optimized structures and calculated coordination energies. (**a**) Optimized structures of perfectly planar C_{2v} Ni∈B_{18} (**1**) and cage-like C_s Ni∈B_{40} (**2**), C_2 Ni_2∈B_{18} (**3**), C_s Ni_3∈B_{40} (**4**), and D_{2d} Ni_4∈B_{40} (**5**) at PBE0/6-311 + G* level. (**b**) Calculated coordination energies (E_c) of the Ni_n∈B_{40} heteroborospherenes with respect to $Ni_nB_{40} = Ni_{(n-1)}B_{40} + Ni$ (n = 1–6).The optimized structures of the C_{2v} Ni_5∈B_{40} (**8**) and D_{2d} Ni_6∈B_{40} (**9**) are depicted in Fig. S2.

Molecular Dynamics Simulations. Extensive molecular dynamics simulations were performed on Ni∈B_{40} (**2**) and Ni_2∈B_{40} (**3**) for 30 ps to allow for crossing of small energy barriers at finite temperatures (Figs S7 and S8). As shown in Figs S7 and S8, both of them are dynamically stable at 500 K, with the root-mean-square-deviation and maximum bond length deviation values of RMSD = 0.07 Å, 0.08 Å and MAXD = 0.25 Å, 0.25 Å, respectively. The two species remain dynamically stable at 700 K, with RMSD = 0.09 Å, 0.09 Å and MAXD = 0.31 Å, 0.31 Å. However, at 1000 K, C_s Ni∈B_{40} (**2**) starts to hop between the two lowest-lying C_s and C_1 isomers with RMSD = 0.15 Å and MAXD = 0.66 Å, while C_2 Ni_2∈B_{40} (**3**) still keeps its structural integrity.

Bonding Analyses. The high stabilities of these heteroborospherenes originate from their electronic structures and bonding patterns. We performed detailed adaptive natural density partitioning (AdNDP)[57,58] analyses on the perfectly planar Ni∈B_{18} (**1**) and cage-like Ni∈B_{40} (**2**) (Fig. 2) which show obvious similarity in bonding patterns though the η^7-B_7 heptagon in the latter is slightly off-planed on the cage surface. The phNi center in Ni∈B_{40} (**2**) forms three lone pairs in radial direction ($3d_z^2$, $3d_{xz}^2$, *and* $3d_{yz}^2$) with the occupation numbers of |ON| = 1.81–1.94 |e| and two nearly in-plane 8c-2e σ-coordination bonds between the remaining tangential Ni 3d orbitals (3_{x2-y2} *and* $3d_{xy}$) and the η^7-B_7 heptagon around it with |ON| = 1.86 |e|. The 48 delocalized σ bonds (40 3c-2e and 8 6c-2e) and 12 delocalized π bonds (4 5c-2e, 4 6c-2e, and 4 7c-2e) on the boron framework in Ni∈B_{40} (**2**) (Fig. 2b) are basically inherited from the parent D_{2d} B_{40}[22]. A similar bonding pattern exists in Ni∈B_{18} (**1**) in which the phNi center carries three lone pairs ($3d_z^2$, $3d_{xz}^2$, *and* $3d_{yz}^2$) in vertical direction with |ON| = 1.83–1.99 |e| and forms two perfectly in-plane 8c-2e σ-coordination bonds with the η^7-B_7 heptagon around it with |ON| = 1.80–1.85 |e|, with 22 σ bonds (13 2c-2e, 2 3c-2e, and 7 4c-2e) and 5 4c-2e π bonds on the boron framework outside. Natural bonding orbital (NBO) analyses indicate that the phNi centers in Ni∈B_{18} (**1**) and Ni∈B_{40} (**2**) possess the electronic configurations of $[Ar]4s^{0.00}3d^{9.26}$ and $[Ar]4s^{0.17}3d^{9.34}$, natural atomic charges of + 0.48 |e| and + 0.47 |e|, and total Wiberg bond orders of 1.78 and 1.59, respectively. These results show that the phNi center in **1** and **2** donates its $4s^2$ electrons almost completely to the boron framework and, in return, accepts about the same amount of electrons in its partially occupied *3d* tangential orbitals (3_{x2-y2} and $3d_{xy}$) from the η^7-B_7 heptagon via effective $p \rightarrow d$ back-donations. The phNi centers in **1** and **2** have therefore approximately the total bond order of two corresponding to the two 8c-2e σ-coordination bonds between phNi and its η^7-B_7 ligand. Such a bonding pattern exists in other phNi-doped Ni_n∈B_{40} heteroborospherenes (n = 2–4) as well (Figs S9–11). The double delocalization bonding pattern on the B_{40} framework renders 3D aromaticity to these heteroborospherenes, as evidenced by the negative calculated nucleus independent chemical shift (NICS)[59] values of −43.1, −43.4, −42.4, and −42.2 ppm at the cage centers of Ni∈B_{40} (**2**), Ni_2∈B_{40} (**3**), Ni_3∈B_{40} (**4**), and Ni_4∈B_{40} (**5**), respectively, which are well comparable with the corresponding value of −43 ppm calculated for D_{2d} B_{40}[22].

IR, Raman, and UV-vis spectra. We computationally simulate the IR, Raman, and UV-vis absorption spectra of C_{2v} Ni∈B_{18} (**1**) (Fig. S12) and C_s Ni∈B_{40} (**2**) (Fig. 3 and Fig. S13) to facilitate their spectral characterizations. With major IR peaks at 1276 cm^{-1}(a'), 1153 cm^{-1} (a"), 783 cm^{-1} (a'), 566 cm^{-1} (a'), and 368 cm^{-1} (a") and Raman peaks at 1320 cm^{-1} (a'), 1161 cm^{-1} (a'), 646 cm^{-1} (a'), 432 cm^{-1} (a'), 182 cm^{-1} (a'), and 148 cm^{-1} (a') (Fig. 3), Ni∈B_{40} (**2**) exhibits similar spectral features with the parent D_{2d} B_{40} and D_{2d} B_{40}^+[24,25,60]. These IR and Raman active modes mainly originate from the vibrational transitions of the B_{40} framework. The Raman peaks at 182 cm^{-1} (a') and 148 cm^{-1} (a') represent typical radial breathing modes (RBMs) of the C_s Ni∈B_{40} (**2**) cage in two perpendicular directions. An intense peak at 210 cm^{-1} was used to characterize the hollow structure of

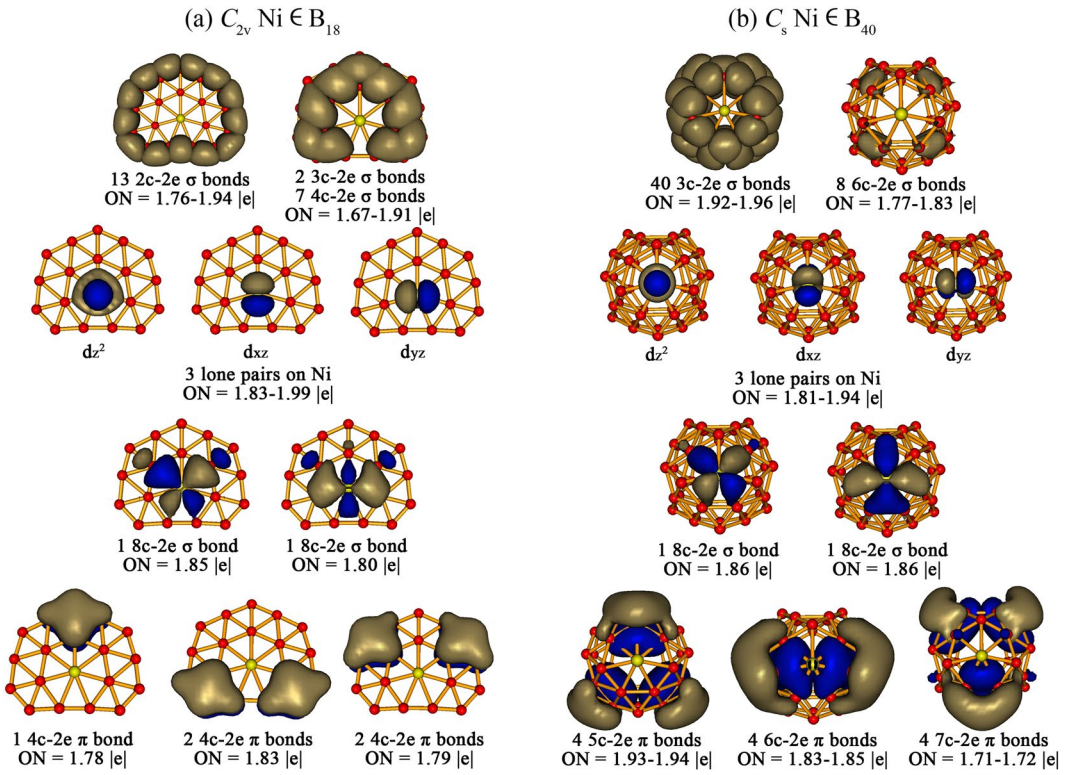

Figure 2. Comparison of the AdNDP bonding patterns of (**a**) C_{2v} Ni ∈ B_{18} (**1**) and (**b**) C_s Ni ∈ B_{40} (**2**).

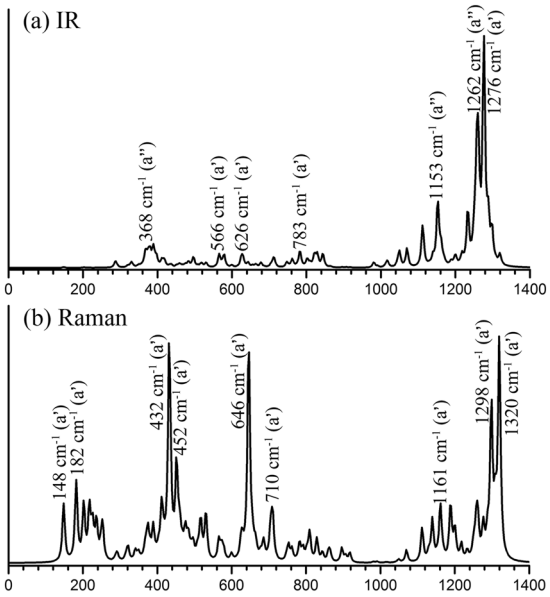

Figure 3. Simulated (**a**) IR and (**b**) Raman spectra of C_s Ni ∈ B_{40} (**2**) at PBE0/6-311 + G* level.

single-walled boron nanotubes[61]. The simulated UV-vis absorption spectroscopy of Ni ∈ B_{40} (**2**) (Fig. S13) using the time-dependent DFT approach[62] also exhibits certain similarity with that of D_{2d} B_{40}, with the main spectral features located at 201, 217, 242, 275, 301, 324, 415, 501, and 622 nm. Most of the strong absorptions originate from electronic transitions from the deep inner shells to high-lying unoccupied molecular orbitals of the neutral, with the weak absorptions above 500 nm involving transitions from frontier orbitals with Ni *3d* contributions. We also simulated the photoelectron spectra (PES) of the cage-like C_s Ni ∈ B_{40}^-, C_2 Ni_2 ∈ B_{40}^-, C_s Ni_3 ∈ B_{40}^-, and D_{2d} Ni_4 ∈ B_{40}^- monoanions (Fig. S14) which appear to have the low calculated first vertical and adiabatic

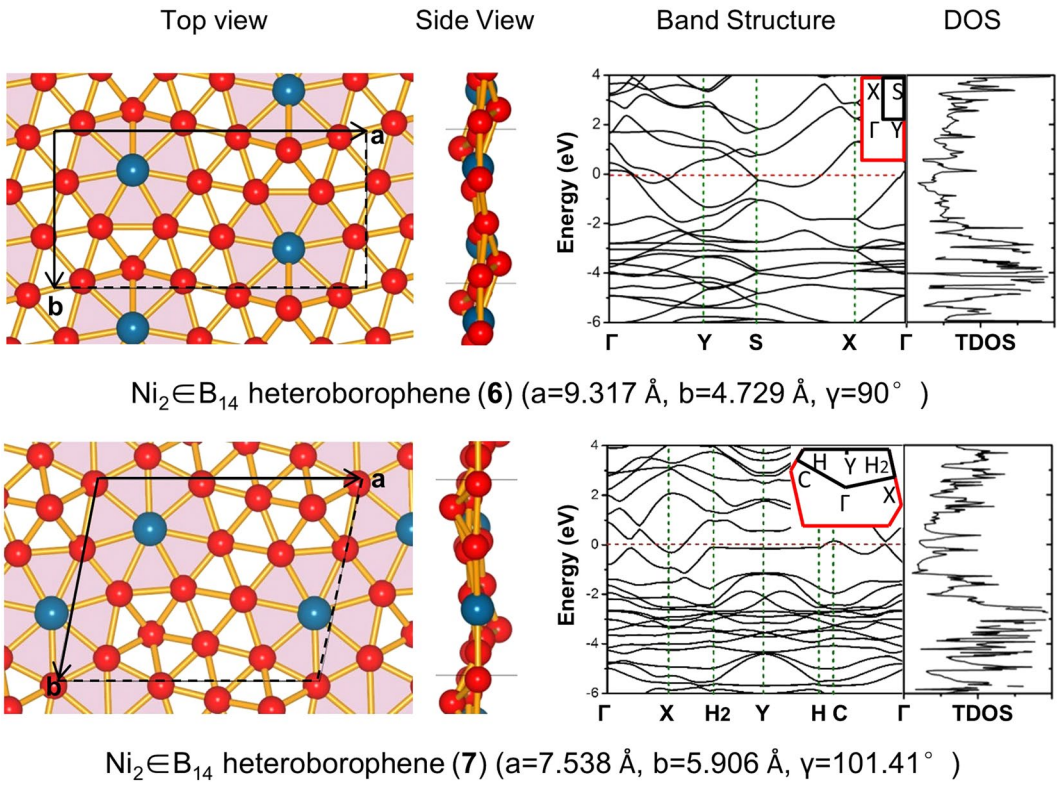

Figure 4. Top and side views of the structures of 2D heteroborophenes. $Ni_2 \in B_{14}$ (**6**) and $Ni_2 \in B_{14}$ (**7**) were optimized at PBE and their band structures and total densities of states (TDOS) were calculated at HSE06. The insets represent the shapes of first Brillouin zones. Γ, X, A and Z of (**6**) correspond to the (0, 0, 0), (0, 0.5, 0), (0.5, 0.5, 0) and (0.5, 0, 0) k-points, while Γ, X, H_2, Y, H and C of (**7**) correspond to the (0, 0, 0), (0.5, 0, 0), (0.440, 0.389, 0), (0, 0.5, 0), (−0.440, 0.611, 0) and (−0.5, 0.5, 0) k-points.

detachment energies of VDE/ADE = 2.40/2.30, 2.39/2.29, 2.40/2.32, and 2.34/2.26 eV, respectively, followed by a sizable energy gap of about 1.0 eV, similar to the measured PES of the cage-like D_{2d} B_{40}^- [22].

Heteroborophene monolayers $Ni_2 \in B_{14}$ (6, 7). To locate the planar monolayer precursor of the cage-like heteroborospherenes (**2**–**5**), we performed an extensive GM search on a Ni_2B_{14} monolayer which contains a unit cell doubling the size of a planar NiB_7 coordination unit. With more than 950 valid structures probed, the nearly degenerate $Ni_2 \in B_{14}$ (**6**) ($P2_1/m$) and $Ni_2 \in B_{14}$ (**7**) (*P-1*) monolayers (Fig. 4) which may coexist in experiments turn out to be the two lowest-lying 2D polymorphs of the system (Fig. S15) without imaginary phonon dispersion frequencies at PBE level[54] (Fig. S16). Slight buckling occurs in these heteroborophene monolayers with the maximum buckled heights of 1.16 Å in **6** and 1.51 Å in **7** at the pentacoordinate B sites, similar to the symmetric buckling observed in silicene[63]. $Ni_2 \in B_{14}$ (**6**) and $Ni_2 \in B_{14}$ (**7**) possess the average cohesive energies of $E_{coh} = 5.932$ eV and 5.939 eV per atom ($E_{coh} = (2E_{Ni} + 14E_B - E_{Ni2B14})/16$), respectively, which are higher than the cohesive energies of the recently proposed FeB_6 (5.79 eV/atom) and FeB_2 (4.87 eV/atom) at the same theoretical level[37,38]. The current prediction of heteroborophene monolayers **6** and **7** with nearly in-plane phNi centers is supported by the recently observed perfectly planar heteroborophene-type $Co \in B_{18}^-$ cluster which contains a phCo center[39]. More intriguingly, the $Ni_2 \in B_{14}$ (**6**) monolayer composed of interwoven BDCs with two equivalent phNi centers per unit cell turns out to be the precursor of the cage-like heteroborospherenes (**2**–**5**) which, with four heptagons on the waist and two hexagons at the top and bottom, can be unfolded into $Ni_2 \in B_{14}$ (**6**) monolayer by repetition simultaneously along the orthogonal direction (Fig. S17). This observation builds an interesting link between heteroborophene monolayers and cage-like heteroborospherenes. Lying 0.007 eV/atom higher in cohesive energy than $Ni_2 \in B_{14}$ (**6**), $Ni_2 \in B_{14}$ (**7**) with both capped pentagons (B_6) and hexagons (B_7) also contains two equivalent phNi centers per unit cell. Both $Ni_2 \in B_{14}$ (**6**) and $Ni_2 \in B_{14}$ (**7**) monolayers turn out to be metallic in nature, as shown in their calculated band structures and total densities of states (Fig. 4) which possess non-zero densities at Fermi levels, similar to boron α-sheet and other low-lying boron monolayers[34–36]. Detailed SSAdNDP bonding analyses[57,58] (Fig. S18) show that both $Ni_2 \in B_{14}$ (**6**) and $Ni_2 \in B_{14}$ (**7**) possess a σ + π double delocalization bonding pattern on their boron frameworks, with each phNi center forming three lone pairs ($3d_z^2$, $3d_{xz}^2$, *and* $3d_{yz}^2$) in vertical direction and two nearly in-plane 8c-2e σ-coordination bonds with the η^7-B_7 pentagon around it. Such a bonding pattern is well in line with the bonding patterns in both planar $Ni \in B_{18}$ (**1**) and cage-like $Ni_n \in B_{40}$ (n = 1–4) (**2**–**5**) discussed above. The σ + π double delocalization bonding pattern on the boron frameworks renders metallicity to these 2D heteroborophenes.

In summary, based on extensive first-principles calculations, we have presented the possibility of the novel planar heteroborophene-type cluster $Ni \in B_{18}$ (**1**), 3D aromatic heteroborospherenes $Ni_n \in B_{40}$ (n = 1–4) (**2**–**5**), and 2D metallic heteroborophenes $Ni_2 \in B_{14}$ (**6, 7**) which all contain phNi centers in η^7-B_7 pentagons with the universal bonding pattern of $\sigma + \pi$ double delocalization on their boron frameworks, with each phNi forming two effective 8c-2e σ-coordination bonds with the η^7-B_7 heptagon around it. Initial investigations suggest that phNi centers in **2**–**7** can be substituted by phPd, phPt, or other phTM dopants with the right atomic radii and electronic configurations to form stable heteroborospherenes, heteroborophenes, and heteroboronanotubes. Possible free-standing heteroboronanostructures stabilized by phTM centers guarantee further experimental and theoretical investigations to expand the chemistry and materials science of boron which are expected to be complementary to that of carbon[31–38].

References

1. Kroto, H. W., Heath, J. R., O'Brien, S. C., Curl, R. F. & Smalley, R. E. C_{60}: Buckminsterfullerene. *Nature* **318**, 162–163 (1985).
2. Novoselov, K. S. *et al*. Electric eield effect in atomically thin carbon films. *Science* **306**, 666–669 (2004).
3. Cotton, F. A., Wilkinson, G., Murillo, C. A.& Bochmann, M. Advanced Inorganic Chemistry, 6th Edn., Wiley, New York (1999).
4. Zhai, H.-J., Kiran, B., Li, J. & Wang, L.-S. Hydrocarbon analogues of boronclusters–planarity, aromaticity and antiaromaticity. *Nat. Mater.* **2**, 827–833 (2003).
5. Kiran, B. *et al*. Planar-to-tubular structural transition in boronclusters: B_{20} as the embryo of single-walled boron nanotubes. *Proc. Natl. Acad. Sci. USA* **102**, 961–964 (2005).
6. Huang, W. *et al*. A concentric planar doubly p-aromatic B_{19}^- cluster. *Nat. Chem.* **2**, 202–206 (2010).
7. Oger, E. *et al*. Boron cluster cations: transition from planar to cylindrical structures. *Angew. Chem. Int. Ed.* **46**, 8503–8506 (2007).
8. Li, W.-L., Zhao, Y.-F., Hu, H.-S., Li, J. & Wang, L.-S. $[B_{30}]^-$: A quasi planar chiral boron cluster. *Angew. Chem. Int. Ed.* **53**, 5540–5545 (2014).
9. Li, W.-L. *et al*. The B_{35} Cluster with a double-hexagonal vacancy: anew and more flexible structural motif for borophene. *J. Am. Chem. Soc.* **136**, 12257–12260 (2014).
10. Piazza, Z. A. *et al*. Planar hexagonal B_{36} as a potential basis for extended single-atom layer boron sheets. *Nat. Commun.* **5**, 3113 (2014).
11. Chen, Q. *et al*. Quasi-planar aromatic B_{36} and B_{36}^- clusters: all-boron analogues of coronene. *Phys. Chem. Chem. Phys.* **16**, 18282–18287 (2014).
12. Alexandrova, A. N., Boldyrev, A. I., Zhai, H.-J. & Wang, L.-S. All-boron aromatic clusters as potential new inorganic ligands and building blocks in chemistry. *Coord. Chem. Rev.* **250**, 2811–2866 (2006).
13. Romanescu, C., Galeev, T. R., Li, W.-L., Boldyrev, A. I. & Wang, L.-S. Aromatic metal-centered monocyclic boron rings: $Co©B_8^-$ and $Ru©B_9^-$. *Acc. Chem. Res.* **46**, 350–358 (2013).
14. Sergeeva, A. P. *et al*. Understanding boron through size-Selected clusters: structure, chemical bonding, and fluxionality. *Acc. Chem. Res.* **47**, 1349–1358 (2014).
15. Wang, L.-S. Photoelectron spectroscopy of size-selected boron clusters: from planar structures to borophenes and borospherences. *Int. Rev. Phys. Chem.* **35**, 69–142 (2016).
16. Luo, X.-M. *et al*. B_{26}^-: The smallest planar boron cluster with a hexagonal vacancy and a complicated potential landscape. *Chem. Phys. Lett.*, doi:10.1016/j.cplett.2016.12.051 (2016).
17. Wang, Y.-J. *et al*. Observation and characterization of the smallest borospherene, B_{28}^- and B_{28}. *J. Chem. Phys.* **144**, 064307 (2016).
18. Li, H.-R. *et al*. Competition between quasi-planar and cage-like structures in the B_{29}^- cluster: photoelectron spectroscopy and *ab initio* calculations. *Phys. Chem. Chem. Phys.* **18**, 29147–29155 (2016).
19. Szwacki, N. G., Sadrzadeh, A. & Yakobson, B. I. B_{80} fullerene: an *ab initio* prediction of geometry, stability, and electronic structure. *Phys. Rev. Lett.* **98**, 166804 (2007).
20. Li, F.-Y. *et al*. B_{80} and $B_{101-103}$ clusters: Remarkable stability of the core-shell structures established by validated density functionals. *J. Chem. Phys.* **136**, 074302 (2012).
21. De, S. *et al*. Energy Landscape of Fullerene Materials: A comparison of boron to boron nitride and carbon. *Phys. Rev. Lett.* **106**, 225502 (2011).
22. Zhai, H.-J. *et al*. Observation of an all-boron fullerene. *Nat. Chem.* **6**, 727–731 (2014).
23. Chen, Q. *et al*. Experimental and theoretical evidence of an axially chiral borospherene. *ACS Nano* **9**, 754–760 (2015).
24. Chen, Q. *et al*. Cage-Like B_{41}^+ and B_{42}^{2+}: New chiral members of the borospherene family. *Angew. Chem. Int. Ed.* **54**, 8160–8164 (2015).
25. Li, H.-R. *et al*. Cage-like B_{40}^+: a perfect borospherene monocation. *J. Mol. Model.* **22**, 124 (2016).
26. Chen, Q. *et al*. Endohedral Ca@B_{38}: stabilization of a B_{38}^{2-} borospherene dianion by metal encapsulation. *Phys. Chem. Chem. Phys.* **18**, 11610–11615 (2016).
27. Chen, Q. *et al*. Endohedral charge-transfer complex $Ca@B_{37}^-$: stabilization of a B_{37}^{3-} borospherene trianion by metal-encapsulation. *Phys. Chem. Chem. Phys.* **18**, 14186–14190 (2016).
28. Tian, W.-J. *et al*. Saturn-like charge-transfer complexes $Li_4\&B_{36}$, $Li_5\&B_{36}^+$, and $Li_6\&B_{36}^{2+}$: exohedral metalloborospherenes with a perfect cage-like B_{36}^{4-}. *Phys. Chem. Chem. Phys.* **18**, 9922–9926 (2016).
29. Bai, H., Chen, Q., Zhai, H.-J. & Li, S.-D. Endohedral and exohedral metalloborospherenes: $M@B_{40}$ (M = Ca,Sr) and $M\&B_{40}$ (M = Be, Mg). *Angew. Chem. Int. Ed.* **54**, 941–945 (2015).
30. Jin, P., Hou, Q.-H., Tang, C.-C. & Chen, Z.-F. Computational investigation on the endohedral borofullerenes $M@B_{40}$ (M = Sc,Y, La). *Theor Chem Acc* **134**, 13, doi:10.1007/s00214-014-1612-4 (2015).
31. Mannix, A. J. *et al*. Synthesis of borophenes: anisotropic, two-dimensional boron polymorphs. *Science* **350**, 1513–1514 (2015).
32. Feng, B.-J. *et al*. Experimental realization of two-dimensional boron sheets. *Nat. Chem.* **8**, 563–568 (2016).
33. Yang, Y., Zhang, Z.-H., Penev, E. S. & Yakobson, B. I. B_{40}: stability and planar structural precursor. *Nanoscale* **9**, 1805–1810 (2017).
34. Tang, H. & Ismail-Beigi, S. Novel precursors for boron nanotubes: the competition of two-center and three-center bonding in boron sheets. *Phys. Rev. Lett.* **99**, 115501 (2007).
35. Penev, E. S., Bhowmick, S., Sadrzadeh, A. & Yakobson, B. I. Polymorphism of two-dimensional boron. *Nano Lett.* **12**, 2441–2445 (2012).
36. Lu, H.-G., Mu, Y.-W., Bai, H., Chen, Q. & Li, S.-D. Binary nature of monolayer boron sheets from *ab initio* global searches. *J. Chem. Phys.* **138**, 024701 (2013).
37. Zhang, H.-J., Li, Y.-F., Hou, J.-H., Du, A.-J. & Chen, Z.-F. Dirac state in the FeB_2 monolayer with graphene-like boron sheet. *Nano Lett.* **16**, 6124–6129 (2016).
38. Zhang, H.-J., Li, Y.-F., Hou, J.-H., Tu, K.-X. & Chen, Z.-F. FeB_6 Monolayers: the graphene-like material with hypercoordinate transition metal. *J. Am. Chem. Soc.* **138**, 5644–5651 (2016).
39. Li, W.-L. *et al*. The planar CoB_{18}^- cluster as a motif for metallo-borophenes. *Angew. Chem. Int. Ed.* **55**, 7358–7363 (2016).

40. Goedecker, S. Minima hopping: an efficient search method for the global minimum of the potential energy surface of complex molecular systems. *J. Chem. Phys.* **120**, 9911–9917 (2004).
41. Goedecker, S., Hellmann, W. & Lenosky, T. Global minimum determination of the Born-Oppenheimer surface within density functional theory. *Phys. Rev. Lett.* **95**, 055501 (2005).
42. Chen, X., Zhao, Y.-F., Wang, L.-S. & Li, J. Recent progresses of global minimum search of nanoclusters with a constrained Basin-Hopping algorithm in the TGmin program. *Comput. Theor. Chem.* **1107**, 57–65 (2017).
43. Adamo, C. & Barone, V. Toward reliable density functional methods without adjustable parameters: the PBE0 model. *J. Chem. Phys.* **110**, 6158–6170 (1999).
44. Tao, J., Perdew, J. P., Staroverov, V. N. & Scuseria, G. E. Climbing the density functional ladder: nonempirical meta-generalized gradient approximation designed for molecules and solids. *Phys. Rev. Lett.* **91**, 146401 (2013).
45. Krishnan, R., Binkley, J. S., Seeger, R. & Pople, J. A. Self-consistent molecular orbital methods. XX. A basis set for correlated wave functions. *J. Chem. Phys.* **72**, 650 (1980).
46. Čížek, J. On the use of the cluster expansion and the technique of diagrams in calculations of correlation effects in atoms and molecules. *Adv. Chem. Phys.* **14**, 35–89 (1969).
47. Purvis, G. D. & Bartlett, R. J. A full coupled-cluster singles and doubles model: The inclusion of disconnected triples. *J. Chem. Phys.* **76**, 1910–1918 (1982).
48. Raghavachari, K., Trucks, G. W., Pople, J. A. & Head-Gordon, M. A fifth-order perturbation comparison of electron correlation theories. *Chem. Phys. Lett.* **157**, 479–483 (1989).
49. Wang, Y.-C., Lv, J., Zhu, L. & Ma, Y.-M. Crystal structure prediction via particle-swarm optimization. *Phys. Rev. B* **82**, 094116 (2010).
50. Kresse, G. & Furthmuller, J. Efficient iterative schemes for ab initio total-energy calculations using a plane-wave basis set. *J. Phys. Rev. B* **54**, 11169–11186 (1996).
51. Kresse, G. & Hafner, J. Norm-conserving and ultrasoft pseudopotentials for first-row and transition elements. *J. Phys. Condens. Matter* **6**, 8245–8257 (1994).
52. Blochl, P. E. Projector augmented-rave method. *Phys. Rev. B* **50**, 17953–17979 (1994).
53. Kresse, G. & Joubert, D. From ultrasoft pseudopotentials to the projector augmented-wave method. *Phys. Rev. B* **59**, 1758–1775 (1999).
54. Perdew, J. P., Burke, K. & Ernzerhof, M. Generalized gradient approximation made simple. *Phys. Rev. Lett.* **77**, 3865–3868 (1996).
55. Heyd, J., Scuseria, G. E. & Ernzerhof, M. Hybrid functionals based on a screened coulomb potential. *J. Chem. Phys.* **118**, 8207–8215 (2003).
56. Pyykkö, P. Additive covalent radii for single-, double-, and triple-bonded molecules and tetrahedrally bonded crystals: a summary. *J. Phys. Chem. A* **119**, 2326–2337 (2015).
57. Zubarev, D. Y. & Boldyrev, A. I. Developing paradigms of chemical bonding: adaptive natural density partitioning. *Phys. Chem. Chem. Phys.* **10**, 5207–5217 (2008).
58. Galeev, T. R., Dunnington, B. D., Schmidt, J. R. & Boldyrev, A. I. Solid state adaptive natural density partitioning: a tool for deciphering multi-center bonding in periodic systems. *Phys. Chem. Chem. Phys.* **15**, 5022–5029 (2013).
59. Schleyer, P. V. R., Maerker, C., Dransfeld, A., Jiao, H.-J. & Hommes, N. J. V. E. Nucleus-independent chemical shifts: asimple and efficient aromaticity probe. *J. Am. Chem. Soc.* **118**, 6317–6318 (1996).
60. He, R.-X. & Zeng, X.-C. Electronic structures and electronic spectra of all-boron fullerene B_{40}. *Chem Commun.* **51**, 3185–3188 (2015).
61. Ciuparu, D., Klie, R. F., Zhu, Y. M. & Pfefferle, L. Synthesis of pure boron single-wall nanotubes. *J. Phys. Chem. B* **108**, 3967–3969 (2014).
62. Bauernschmitt, R. & Ahlrichs, R. Treatment of electronic excitations within the adiabatic approximation of time dependent density functional theory. *Chem. Phy. Lett.* **256**, 454–464 (1996).
63. Jose, D. & Datta, A. Structures and chemical properties of silicene: unlike graphene. *Acc. Chem. Res.* **47**, 593 (2014).

Acknowledgements

This project was financially supported by the National Natural Science Foundation of China (21373130, 11504213, and 21473106).

Author Contributions

S.-D. Li, H.-G. L., and Y.-W. Mu designed the research. H.-R. Li, X.-X. Tian, X.-M. Luo, and M. Yan performed the calculations. All authors contributed to the interpretation and discussion of the data and participated in the preparation of the manuscript.

Additional Information

Supplementary information accompanies this paper at doi:10.1038/s41598-017-06039-9

Competing Interests: The authors declare that they have no competing interests.

Publisher's note: Springer Nature remains neutral with regard to jurisdictional claims in published maps and institutional affiliations.